# MEASUREMENT OF WATER VAPOR CONCENTRATION USING TUNABLE DIODE LASER ABSORPTION SPECTROSCOPY

A Thesis

by

ALEXANDER BERTRAM BARRETT

Submitted to the Office of Graduate Studies of
Texas A&M University
in partial fulfillment of the requirements for the degree of

MASTER OF SCIENCE

December 2009

Major Subject: Mechanical Engineering

# MEASUREMENT OF WATER VAPOR CONCENTRATION USING TUNABLE DIODE LASER ABSORPTION SPECTROSCOPY

A Thesis

by

ALEXANDER BERTRAM BARRETT

Submitted to the Office of Graduate Studies of
Texas A&M University
in partial fulfillment of the requirements for the degree of

MASTER OF SCIENCE

Approved by:

| | |
|---|---|
| Chair of Committee, | Eric Petersen |
| Committee Members, | Kalyan Annamalai |
| | Adonios Karpetis |
| Head of Department, | Dennis O'Neal |

December 2009

Major Subject: Mechanical Engineering

# ABSTRACT

Measurement of Water Vapor Concentration Using Tunable Diode Laser Absorption Spectroscopy. (December 2009)

Alexander Bertram Barrett, B.S., University of Central Florida

Chair of Advisory Committee: Dr. Eric Petersen

Tunable diode laser spectroscopy and the Beer-Lambert relation has been used to measure the absorption of water vapor both in an absorption cell and in a shock tube. The purpose of this thesis is to develop a laser diagnostic capable of determining species concentration. The correlation between species concentration and absorption is known, and if one is known the other can be calculated. A diode laser was obtained which has a tunable range of 1325.7 - 1400.8 nm and is centered at 1384 nm. An experimental setup was created in which the laser was used to obtain absorption spectroscopy data for water vapor within two separate scenarios- in an absorption cell and in a shock tube. A model was constructed which enabled the calculation of the Voigt profile which in turn was used to determine the absorption coefficient and ultimately enable the utilization of absorption spectroscopy principles to determine species concentration and/or absorption percentage.

The experiments for the absorption cell were performed at room temperature. Twenty runs were performed and the average error for all runs was less than one percent. Three runs were performed for the shock-tube experiments. The absorption was calculated at

three times- prior to the arrival of the shock, after the incident shock passed, and after the reflected shock passed. The temperatures for these conditions were 296K, 1060K, and 2000K respectively. These experiments showed reasonable agreement with theoretical calculations.

# DEDICATION

I'd like to dedicate this thesis to my daughter, Celeste Fay Barrett, and hope that it inspires her to one day pursue her own advanced degree.

# ACKNOWLEDGMENTS

I would like to thank everyone that made it possible for me to complete this work- my advisor, Dr. Eric Petersen, for his support, guidance, and expertise; Chris Aul for helping me complete my experiments in time; my brother, Gil Barrett, for inspiring me to return to college and additionally to pursue graduate work; and last but not least, my wife, Ingrid, whose patience, love, and support made it possible.

# NOMENCLATURE

| | |
|---|---|
| A | area |
| $B_{12}$ | Einstein B coefficient from lower level 1 to upper level 2 [$m^3$ (rad/s) J/s] |
| c | center frequency |
| c | speed of light [m/s] |
| $E_1$ | upper state energy |
| $E_2$ | lower state energy |
| $E_i$ | energy of the quantum state |
| FWHM | full-width at half maximum of the $i^{th}$ perturber |
| $f_B$ | Boltzmann fraction of the absorbing state |
| $g_1$ | electronic degeneracy of levels 1 |
| $g_2$ | electronic degeneracy of levels 2 |
| $g_i$ | internal energy state |
| h | Planck's constant [Js] |
| HWHM | half-width at half maximum of the $i^{th}$ perturber |
| $I_0$ | incident laser intensities |
| $I_0(\omega)$ | incident intensity [$W/m^2$] |
| $I_L(\omega)$ | transmitted intensity [$W/m^2$] |
| $I_T$ | transmitted laser intensities |
| J | rotational quantum number |
| $k_B$ | Boltzmann constant |
| $k_v$ | absorption coefficient [atm $^{-1}cm^{-1}$] |

| | |
|---|---|
| $L$ | path length [cm] |
| $M$ | molecular mass [amu] |
| $N_{abs}$ | number density of absorbers [$m^{-3}$] |
| $N_L$ | Loschmidt number [$m^{-3}atm^{-1}$] |
| $P$ | total pressure [atm] |
| $R$ | internuclear spacing |
| $R_e$ | equilibrium internuclear spacing |
| $Q$ | partition function |
| $S$ | intensity [$cm^{-1}$/ (molecule $cm^{-2}$)] |
| $S_{lu}$ | line strength of the absorption transition [$cm^{-2}atm^{-1}$] |
| $S_{1u}$ | absorption line strength [$m^{-2}$/atm] |
| $T$ | kinetic temperature [K] |
| $v$ | vibrational quantum number |
| wG | Gaussian width |
| wL | Lorentzian width |
| $X$ | mole fraction of the absorber |
| $X_i$ | mole fraction of the $i^{th}$ component |
| $X_{abs}$ | mole fraction of the absorbing species |
| y0 | y-axis offset |
| $\gamma_i$ | HWHM |
| $\nu$ | frequency [$cm^{-1}$] |
| $\nu_0$ | center wavenumber [$cm^{-1}$] |
| $\Phi_\nu$ | lineshape function [cm] |

| | |
|---|---|
| $\Phi(\nu')$ | lineshape function in units of wavenumber |
| $\Phi(\omega)$ | lineshape function of unit area when integrated over frequency [$(rad/s)^{-1}$] |
| $\omega$ | frequency [rad/s] |
| $\hbar$ | reduced Planck constant [J/ (rad/s)] |

# TABLE OF CONTENTS

# LIST OF FIGURES

Page

Page

# CHAPTER I

# INTRODUCTION

The purpose of this thesis is to discuss the details of establishing a tunable laser diagnostic that is capable of determining the concentration of water vapor in various experiments of interest to research being conducted in the Gas Dynamics Laboratory at Texas A&M University. This information is relevant to combustion research for several reasons. Two applications of interest herein include the measurement of water vapor concentration added to a fuel/oxidizer blend before the combustion process and also to measure the water vapor concentration of the products after combustion. The concentration of water vapor can be calculated by using the principles of absorption spectroscopy and the Beer-Lambert relation, which is discussed in more detail in this thesis.

The use of a laser to measure species concentration is of particular concern for combustion experiments because it enables the measurement to be performed without disturbing the flowfield with respect to chemical, physical, or thermofluid parameters. In other words, the pressure, temperature and chemical composition of the environment under observation is not disturbed by the laser absorption diagnostic. Another advantage of laser techniques is that they are not limited to equilibrium situations and can be used to

---

This thesis follows the format of *AIAA Journal*.

measure nonequilibrium environments [1]. Optical diagnostics can provide excellent temporal resolution, providing a way to measure transient occurrences within the flowfield [2].

Laser techniques also have disadvantages. One disadvantage is that the addition of windows entering and leaving the test section is necessary for application of absorption spectroscopy. This involves added complexity to the design. Fortunately, the shock tube used for this thesis already had windows designed into the test section for use as access for diagnostic purposes – for example, a PMT used to measure side wall emission. Another disadvantage is the high cost of tunable lasers, although the appearance of diode lasers has helped considerably in this regard. There is also a fair amount of user knowledge required to set up and operate the diagnostic system, particularly for mechanical engineers with very little or no laser and/or spectrometry coursework [1].

This thesis describes the process of developing a tunable diode laser diagnostic to measure the concentration of water vapor using the principles of absorption spectroscopy. First, a detailed background is given on lasers, optics, and spectroscopy discussing all aspects of the theory required for developing a laser absorption diagnostic. Then, a literature review is given on the history of measuring water vapor concentration with tunable diode laser absorption spectroscopy. Next, the model used in this thesis to implement the principles of absorption spectroscopy is described. The experiment is discussed next and consists of two parts. The first part consists of using a cell as a holding vessel for the water vapor. The second part describes the use of a shock tube as a

holding vessel for the water vapor, which is subsequently exposed to high-temperature conditions behind incident and reflected shock waves. Each part of the experiment is addressed separately with the procedure, experiment, and results presented independently. The conclusion summarizes the data and results for each part of the experiment. Finally, the recommendations section outlines future areas of interest for the extension of the ideas developed in this work.

# CHAPTER II

# BACKGROUND AND PREVIOUS WATER VAPOR ABSORPTION MEASUREMENTS

This section details the theory and reviews the literature relevant to this thesis. The first portion of this section provides the background information on the theory behind this work, starting with lasers and optics and continuing into the fundamentals of absorption spectroscopy. This information is presented in a manner that is conducive to being understood by someone will little or no knowledge in the field of lasers, optics, and spectroscopy. Next, a literature review documents previous work done in relation to laser absorption spectroscopy for water vapor.

## Background

Laser is an acronym which stands for **L**ight **A**mplification by **S**timulated **E**mission of **R**adiation. A laser is a device which emits light, which is electromagnetic radiation, through a process whereby a photon is released by an electron which has been perturbed by a photon of the correct energy [3, 4]. Electromagnetic radiation can be characterized by wavelength and by frequency. These quantities are related to the nature of the wave. Wavelength is the distance between two points on the wave of the same phase. Frequency is the number of oscillations per unit of time. The speed of light in a vacuum is the product of the wavelength and frequency of the light. A third quantity is the wavenumber which is the reciprocal of the wavelength and is a measure of the frequency

and/or energy content of the electromagnetic radiation, usually expressed in units of $cm^{-1}$, or "wavenumbers" [5].

Emission of light occurs when a molecule transitions from a higher excited energy state to lower energy state. In contrast, absorption takes place when a molecule is able to absorb a quantum of energy and transition to a higher energy state. If the lower energy state is sufficiently populated by molecules, there is always a given frequency that is able to stimulate transition from the ground state. Both emission and absorption are governed by Bohr's equation, given as

$$\nu = \frac{E_1 - E_2}{h}, \text{ or } E_2 + h\nu = E_1, \quad (1)$$

where ν is the frequency, $E_1$ is the upper state energy, $E_2$ is the lower state energy, and h is Planck's constant. For absorption, when a photon of frequency ν comes in contact with a molecule of energy $E_2$, the molecule may be able to absorb the photon and its energy will become $E_2 + h\nu$, but only if this higher energy state corresponds to an excited state of that molecule [6].

As a first approximation, the energy of a molecule is represented as the sum of four components. These are the translational, rotational, vibrational, and electronic energies. There are three kinds of spectra- rotational spectra, rotation-vibrational spectra, and electronic spectra. In the rotational spectra, a transition takes place from one rotational level to another rotational level, but remains within the same vibrational and electronic

state. In the rotational-vibrational spectra, a transition takes place from a rotational level of one vibrational level to a rotational level of a different vibrational level. In the electronic spectra a transition occurs from rotational levels within the vibrational levels of one electronic state to the rotational levels within the vibrational levels of a separate electronic state [7].

Figure 1 shows two electronic states of a molecule denoted A and X. The lowest electronic level, or ground state, is the X-state, and the first excited level is the A-state. Within each electronic state are several vibrational states. The vibrational levels are identified by their vibrational quantum numbers, v. Within the lower electronic state, vibrational levels are labeled with a double prime (v"), and the upper electronic state's vibrational levels are labeled with a single prime (v'). Just as the vibrational spacing is smaller than the electronic spacing, the rotational spacing is smaller still. The rotational levels are indicated by their rotational quantum numbers, J. Once again, a double prime denotes a lower level, and a single prime denotes an upper level. The y-axis has units of energy and the x-axis has units of distance, with $R_e$ defined as an equilibrium internuclear spacing and R denoting internuclear spacing. [2]

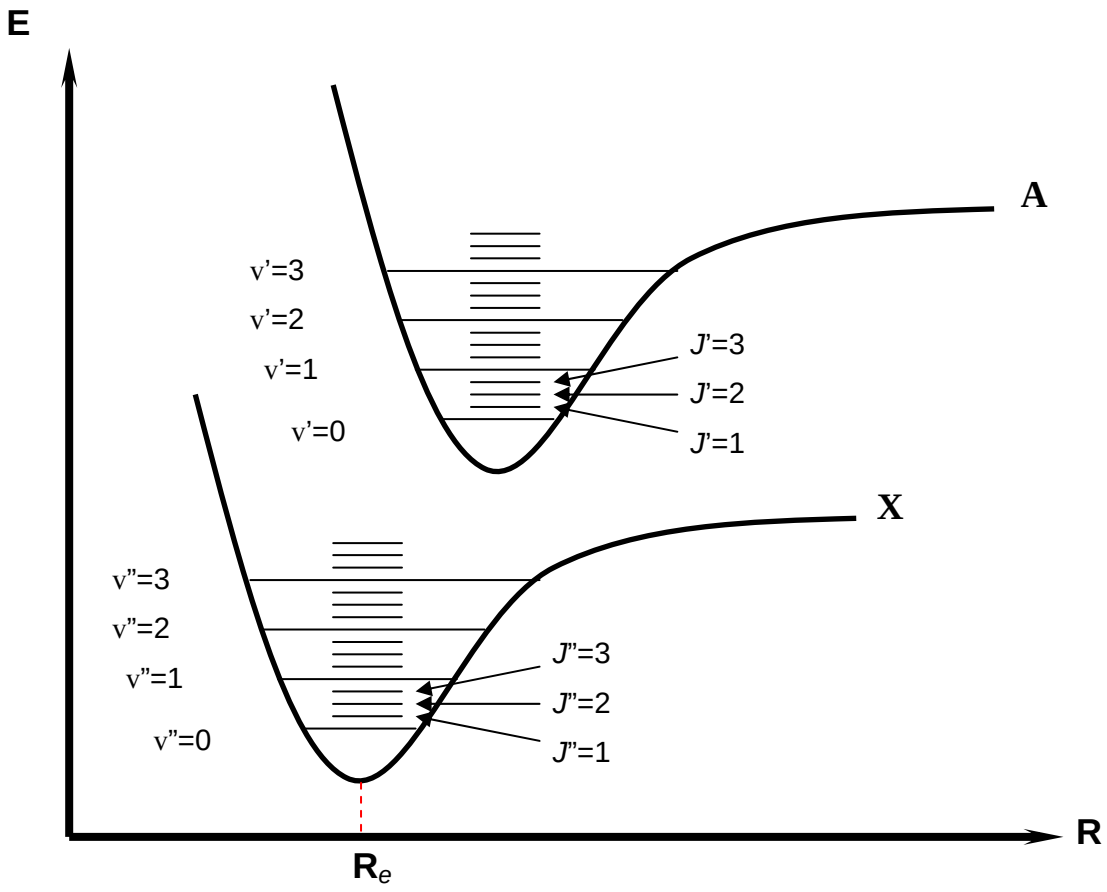


**Figure 1** Schematic diagram for two electronic states of a molecule

The shape of an absorption line, as well as its width, is determined by four factors [6]. An ideal transition would have a single line at the center frequency, but nonideal effects lead to broadening which determine the shape and width of the absorption line. Natural broadening, Doppler broadening, pressure broadening, and electric or magnetic field broadening all influence the shape of the line. Doppler broadening and pressure broadening will be the only broadening effects considered for this work since their effects completely dominate natural and electric (or magnetic) broadening. Natural broadening is a consequence of the limited lifetime of energy states and is an extremely small effect. Electric or magnetic field broadening is not of concern in absorption spectroscopy in the

experiments herein because the absorbing gas must be situated in a strong field or include intense ionization for this effect to be noticed, neither of which is the case. Doppler broadening is an important effect and is due to a frequency shift that is associated with the thermal motion of the molecules of the emitting and absorbing gas [8]. The Doppler, or Gaussian, width is given as

$$\Delta\nu_D = (4 \ln 2)^{0.5} \nu_0 (C_{mp} / c) = 7.16235 (10^{-7}) \nu_0 (T/M)^{0.5}, \quad (2)$$

where $\nu_0$ [$cm^{-1}$] is the center wavelength, $C_{mp}$ is the most probably thermal speed (very much less than the speed of light), c is the speed of light, T [K] is the kinetic temperature, and M [amu] is the molecular mass. Figure 2 shows a typical Gaussian lineshape with the HWHM and centerline frequency illustrated.

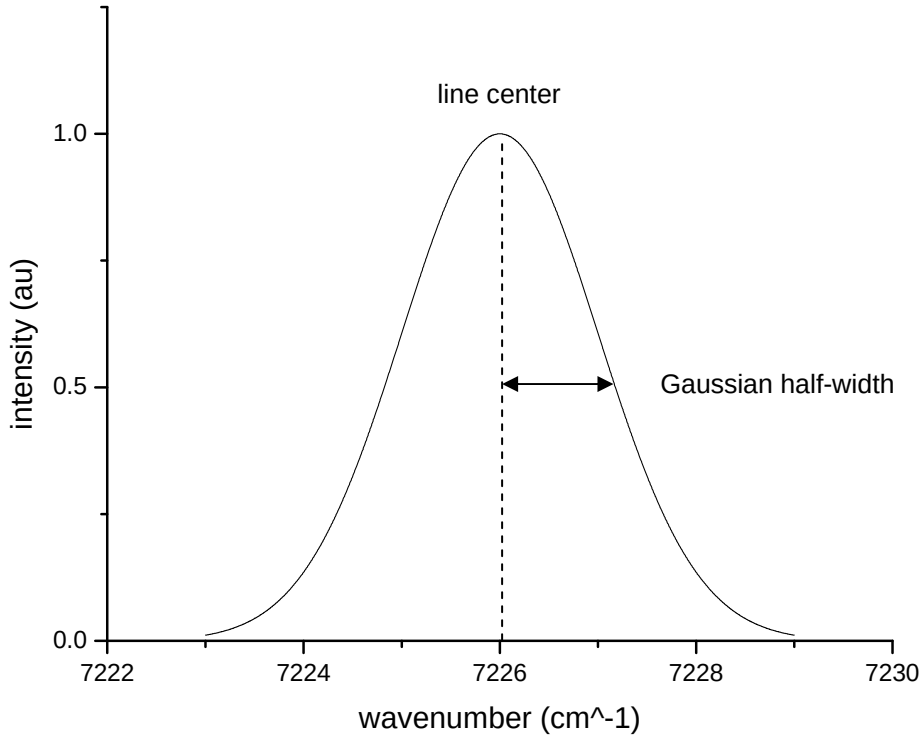


**Figure 2** Gaussian profile showing half-width and center frequency

The pressure, or Lorentzian, broadening is due to the collisions of the molecules of the species of interest with the molecules of other types that are present in the sample. These collisions reduce the lifetime of energy states essentially the same as natural broadening does but to a much greater degree. The Lorentzian, or collision, width is expressed as

$$\Delta\nu_c = P \sum_i (X_i \, 2\gamma_i), \tag{3}$$

where P [atm] is the total pressure, $X_i$ is the mole fraction of the $i^{th}$ component, and $2\gamma_i$ is the FWHM collision width per unit pressure of the $i^{th}$ perturber. Figure 3 shows a typical Lorentzian lineshape with the HWHM and centerline frequency illustrated.

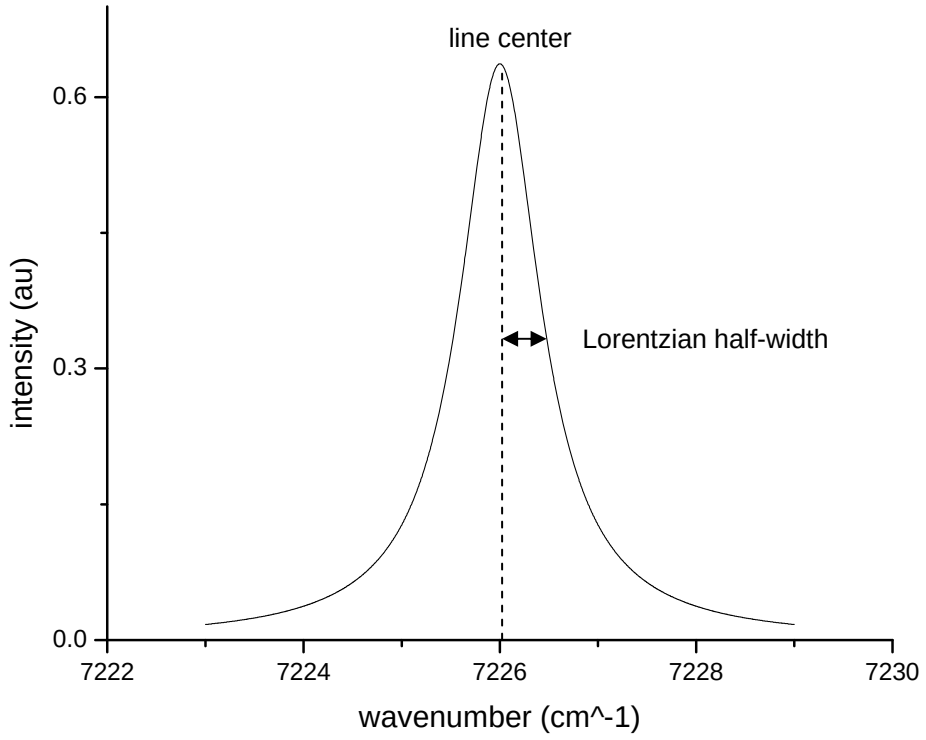


**Figure 3** Lorentzian profile showing half-width and center frequency

Figure 4 illustrates the effect of Lorentzian broadening on a typical lineshape. The original lineshape will be flattened due to the effects of pressure broadening. As the pressure continues to increase, the lineshape will be flattened more.

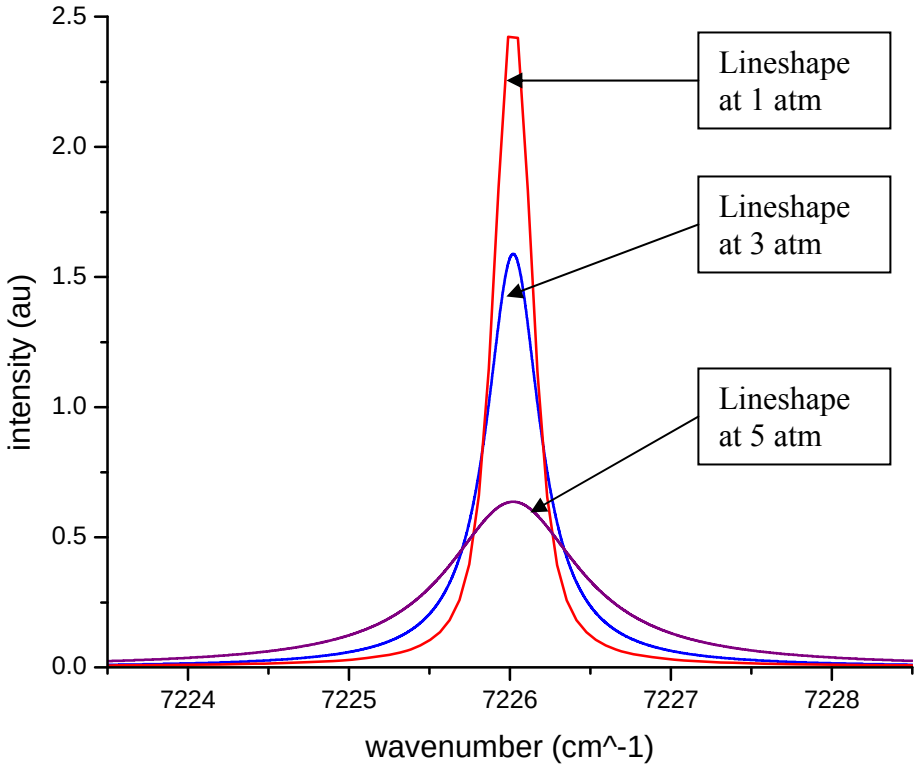


**Figure 4** Effects of pressure broadening on Lorentzian lineshape of water vapor at T = 296K

The Beer-Lambert relation, given as

$$I_T/I_0 = \exp(-k_v P X_{abs} L), \quad (4)$$

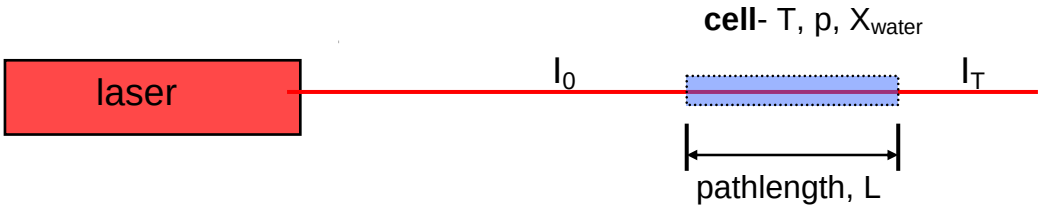


**Figure 5** Illustration of Beer-Lambert relation

can be used to determine the concentration of an individual absorbing species if the pressure, P [atm], path length, L[cm], and absorption coefficient, $k_\nu$ [atm $^{-1}$cm$^{-1}$], are known, as well as the incident, $I_0$, and transmitted, $I_T$, laser intensities. For all calculations, the concentration of water is considered to be uniform. Figure 5 illustrates a generic representation of the Beer-Lambert relation with the laser passing a beam through a cell containing the species of interest. The pressure and path length are easily obtainable. The mole fraction of the absorbing species is denoted as $X_{abs}$. The only other parameter needed to utilize the Beer-Lambert relation is the absorption coefficient, which is somewhat more difficult to determine. The absorption coefficient is discussed in considerable detail in this section, as follows.

The absorption coefficient can be obtained from the expression

$$k_\nu = S_{lu}\, \Phi_\nu, \qquad (5)$$

if the line strength of the absorption transition, $S_{lu}$ [$cm^{-2}atm^{-1}$], and the lineshape function, $\Phi_v$ [cm], are known. The lineshape is normalized such that

$$\int \Phi_v \, dv = 1. \tag{6}$$

The intensity, S [$cm^{-1}$/ (molecule $cm^{-2}$)], can be found in the HITRAN database, but first it was important herein to confirm that this value has the correct units and of the same form as to be used for the purpose of the calculations in this thesis. The procedure to confirm this is discussed next. The Voigt lineshape is burdensome to calculate. It is given by Origin as [9]

$$y = y0 + \frac{2A(\ln 2)wL}{\pi^{1.5} wG^2} \int \frac{e^{-t^2}}{(\sqrt{\ln 2}\,\frac{wL}{wG})^2 + (\sqrt{4\ln 2}\,\frac{x - xc}{wG} - t)^2} \quad . \tag{7}$$

Until recently, there was no closed form solution to the Voigt lineshape function, which is a convolution of the Doppler and Lorentzian broadening [10]. For this work, the lineshape was determined using the Origin software for its ease of use, convenience, and accuracy. The procedure for calculating the Voigt lineshape function is discussed in the next section.

The calculation of the line strength from first principles is an arduous process and requires manipulation of several equations and parameters to reach the final form. As a starting point, consider the equation

$$I_L(\omega) = I_0(\omega) \exp\{-[N_{abs} B_{12} \Phi(\omega) \hbar \omega / c\} L\}, \quad (8)$$

which describes the absorption of monochromatic radiation taking into account a few simplifications such as neglecting thermal equilibrium situations and stimulated emissions [11]. For this equation, $I_L(\omega)$ is the transmitted intensity, $I_0(\omega)$ is the incident intensity (both in units of $W/m^2$), $N_{abs}$ $[m^{-3}]$ is the number density of absorbers, $B_{12}$ $[m^3(rad/s)J/s]$ is the Einstein B coefficient for absorption from lower level 1 to upper level 2, $\Phi(\omega)$ $[(rad/s)^{-1}]$ is the lineshape function of unit area when integrated over frequency, $\hbar$ [J/(rad/s)] is the reduced Planck constant, $\omega$ [rad/s] is the frequency, c [m/s] is the speed of light, and L [m] is the pathlength of the medium. The reduced Planck constant is equal to Planck's constant divided by $2\pi$. It is sometimes called the Dirac constant and is used when frequency is expressed in radians per second rather than cycles per second [12]. The exponential factor of this equation is presented in many forms. One rare, but useful, form is

$$I_L(\nu) = I_0(\nu) \exp\{-[S_{1u} \Phi(\nu') P X] L\}, \quad (9)$$

where $S_{1u}$ [$m^{-2}$/atm] is the absorption line strength, P [atm] is the total pressure, X is the mole fraction of the absorber, $\Phi$ ($\nu$') is the lineshape function in units of wavenumber. The absorption line strength is given by the equation

$$S_{1u}\ [\text{kayser/m/atm}] = N_L\ (273.15/T)\ f_B\ B_{12}\ [\hbar\ \omega\ /\ (2\pi c^2)], \tag{10}$$

where $N_L$ [$m^{-3}atm^{-1}$] is the Loschmidt number, $f_B$ is the Boltzmann fraction of the absorbing state, and T [K] is temperature. The kayser is a unit of frequency equal to a reciprocal meter. The Einstein A coefficient is more readily available than the Einstein B coefficient, so it is more convenient to recast the equation for the absorption strength once more. The Einstein coefficients are related by

$$B_{12} = \frac{g_2}{g_1}\frac{\pi^2 c^3}{\hbar\omega^3}\ A_{21}, \tag{11}$$

where $g_2$ and $g_1$ are the electronic degeneracies of levels 2 and 1, respectively. This conversion is substituted into the previous equation to yield

$$S_{1u}\ [\text{cm}^{-2}/\text{atm}] = N_L\ (273.15/T)\ f_B \frac{g_2}{g_1}\frac{A_{21}}{8\pi c\,\nu^2}, \tag{12}$$

where now frequency, $\nu$, has units of wavenumber [$cm^{-1}$], the speed of light has units of cm/s, and $N_L$ has units of $cm^{-3}atm^{-1}$. If the intensity, S, from the HITRAN database is

multiplied by the Loschmidt number, $N_L$, in units of molecule/ ($cm^3$atm), the result will be $S_{lu}$ in the form of our last equation.

The Boltzmann fraction, $f_B$, is another parameter which must be calculated. The Boltzmann fraction is used to determine what fraction of the total energy is in a particular energy state. The formula used to calculate it is

$$f_B = \frac{g_i e^{\frac{-E_i}{k_B T}}}{Q}, \tag{13}$$

where $g_i$ is the internal energy state, $k_B$ is the Boltzmann constant, $E_i$ is the energy of the quantum state, and Q is the partition function [2]. The values for g and E are taken from the HITRAN database for the ground state of the molecule.

To implement this formula, Q must be also determined and is given as [2]

$$Q = \sum_{tr} \sum_{rot} \sum_{vib} \sum_{elec} (C_{tr} e^{\frac{-E_{trans}}{k_B T}})(g_{rot} e^{\frac{-E_{rot}}{k_B T}})(g_{vib} e^{\frac{-E_{vib}}{k_B T}})(g_{elec} e^{\frac{-E_{elec}}{k_B T}}). \tag{14}$$

Here, once again, we are left with a cumbersome equation which is difficult to implement. However, if we use the rigid-rotor, harmonic-oscillator model, the partition function, Q, is much easier to calculate and is given as [13]

$$Q(T) = 0.5\left[\frac{\pi / ABC}{(kT/hc)^3}\right]^{0.5}\left[1 - e^{(-hc\nu_1/kT)}\right]^{-1}\left[1 - e^{(-hc\nu_2/kT)}\right]^{-1}\left[1 - e^{(-hc\nu_3/kT)}\right]^{-1}. \quad (15)$$

Here A, B, and C are the three rotational constants of an asymmetric top rotor, and $\nu_1$, $\nu_2$, and $\nu_3$ and the three fundamental vibrational frequencies. For water, A, B, and C are equal to 27.0 $cm^{-1}$, 14.4 $cm^{-1}$, and 9.4 $cm^{-1}$, respectively; and $\nu_1$, $\nu_2$, and $\nu_3$ are equal to 3657.05 $cm^{-1}$, 1594.75 $cm^{-1}$, and 3755.93 $cm^{-1}$, respectively [14].

The intensity at specific wavelengths relevant to this thesis was calculated using the procedure described above. These values were then compared to the values given by the HITRAN database. This comparison was performed to ensure a complete understanding of the background and to verify the data in the HITRAN database was of the correct form for usage in this work. In general, the values from the two sources were close in value (<5%). Therefore, the units and form of the parameters in the HITRAN database were deemed appropriate and were employed for the calculations later in this thesis.

Once a value for the intensity of the laser at specific wavelengths has been determined, it can be used to calculate a value for the absorption coefficient. The absorption coefficient can then be used to implement the Beer-Lambert relation.

**Previous Water Vapor Absorption Measurements**

One of the first papers published on measurement of water vapor concentration in a shock tube at elevated temperatures using laser absorption spectroscopy was that by Arroyo and Hanson, 1993 [13]. Water vapor concentration and temperature were measured by tuning the wavelength of a single-mode probe laser across one or more closely spaced spectral lines. The scanned region was from approximately 1383 to 1387 nm. Previously Wang et al. [15] and Goldstein et al. [16] had measured water vapor concentration near 820 nm at room temperature. Carlisle et al. [17] had measured concentration around 1300 nm as did Stanton et al. [18] albeit at higher temperatures. The strongest absorption lines for water at room temperature occur between 1350 and 1410 nm. However, at 1500K, the line strength of the absorption lines between 1340 and 1460 nm are 100 to 1000 times stronger than the lines previously used lying between 820 and 1300 nm [13]. High pressure water vapor spectroscopy has been performed at pressures up to 65 atm and temperatures up to 1800K near 7117, 7185, and 7462 $cm^{-1}$ [19].

# CHAPTER III

# MODEL

This section gives a description of the method used to incorporate the principles of absorption spectroscopy to determine water vapor concentration. A detailed explanation of the exact method used to apply the Beer-Lambert relation is also given. The procedure used in the Origin software to determine the Voigt function for use in the calculation of the absorption coefficient is also documented.

Before calculations for the water vapor concentration can be performed, the absorption coefficient has to be calculated. But, to determine the absorption coefficient, the lineshape function first has to be determined. Thus, calculating the Voigt lineshape for the water line of interest is the starting point for the spectroscopy calculations. Although there are several researchers who have solved the Voigt profile function in closed form [20, 21], for this work, the lineshape function was determined using the Origin software, as mentioned in Chapter II. The Origin function makes the calculation much easier and was very time saving since the Voigt profile had to be calculated several times for this work. Origin has a built-in Voigt lineshape function curve simulation feature. To utilize this feature, five parameters are needed. These are y0, c, A, wG, and wL, which are the y-axis offset, center frequency, area, Gaussian width, and Lorentzian width, respectively. Since we have normalized the area to unity, A will always be equal to one. The center frequency, y0, is set to the center wavelength (or wavenumber) of interest. The y-axis

offset is always set to zero. The Gaussian width and the Lorentzian width can both be determined. The Gaussian width is calculated using the equation

$$wG = 7.16235\times10^{-7}\ \nu_0\ (T/M)^{0.5}, \quad (16)$$

where $\nu_0$ is the center wavenumber in units of $cm^{-1}$, T is the temperature in units of Kelvin, and M is the molecular mass in units of amu. The Lorentzian width is calculated from the equation

$$wL = P \sum_i (X_i\ 2\gamma_i), \quad (17)$$

where P is the total pressure in atmospheres, $X_i$ is the mole fraction of the $i^{th}$ perturber, and $\gamma_i$ is the HWHM, half-width at half maximum of the $i^{th}$ perturber. Figure 6 shows a picture of the Voigt function initialization as seen in Origin. This screen shows the five parameters that are needed to determine the Voigt lineshape, parameter settings, parameter initialization, and the Voigt function.

Equations (16) and (17) are the same as equations (2) and (3) with the exception that equations (16) and (17) use the Origin nomenclature.

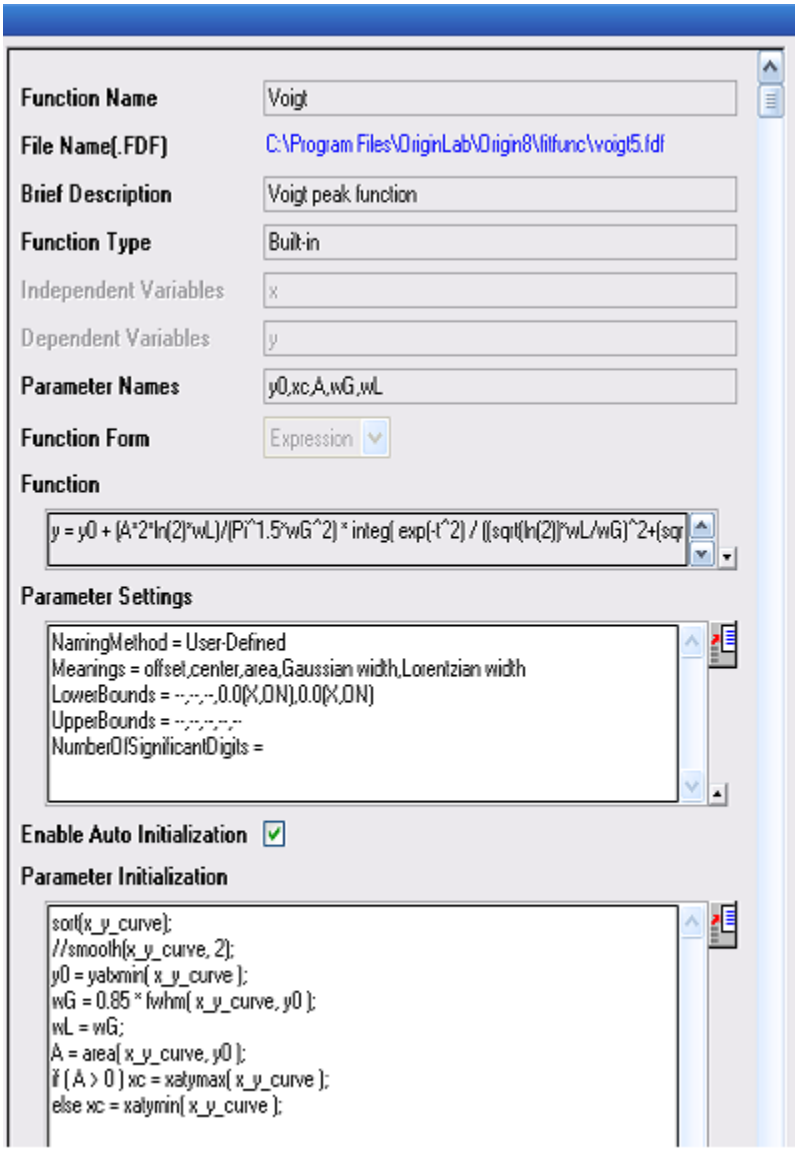


**Figure 6** Origin Voigt function initialization

To create a Voigt curve for a specific spectroscopic line, we click the *analysis* tab, then *fitting*, and finally *simulate curve*. This will bring up the screen shown in Figure 7. This screen gives an option for the specific type of function that will be simulated. Simply click *Voigt*, enter the five parameters, y0, c, A, wG, and wL, set Xminimum and Xmaximum, and include the number of points and the noise level. (For this work, the

noise was left as zero.) A preview of the curve fit is shown in the upper right corner of the screen. Once all the parameters are set, click OK, and a new page will appear showing the simulated curve. Figure 8 shows an example of this curve using arbitrary values.

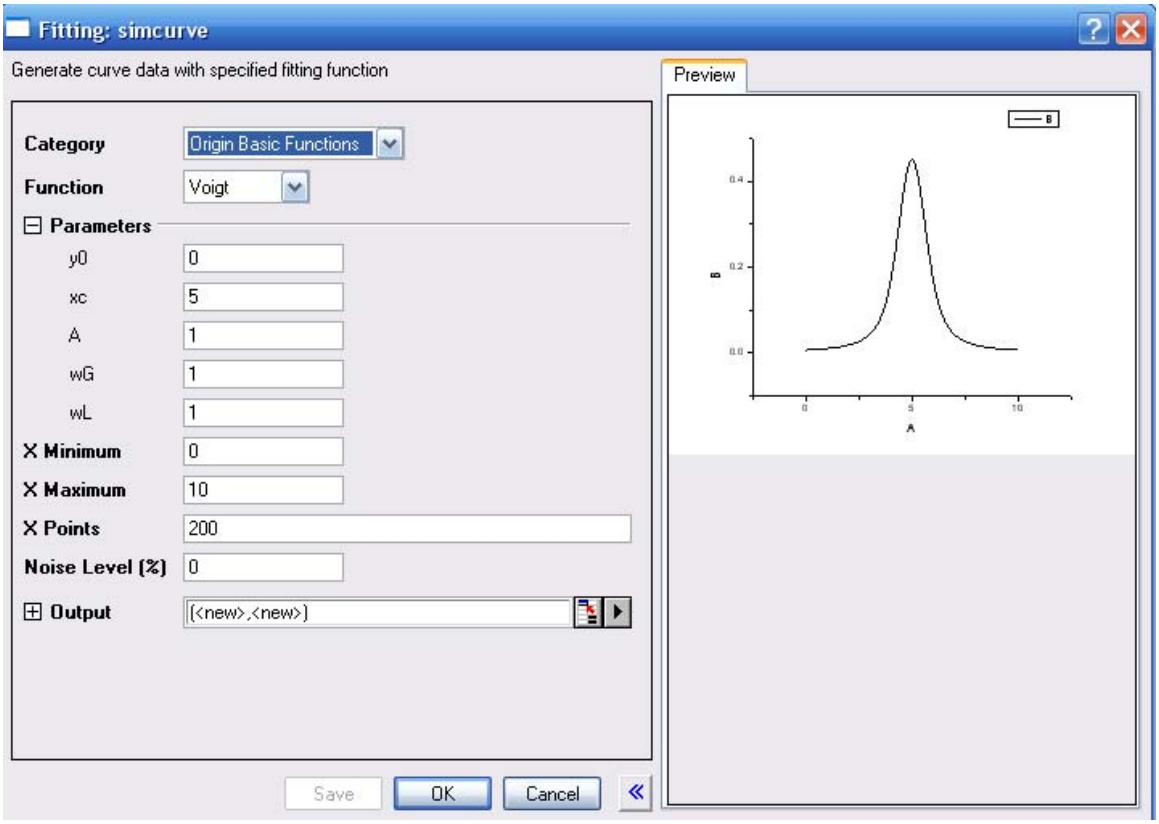


**Figure 7** Origin Voigt curve simulation

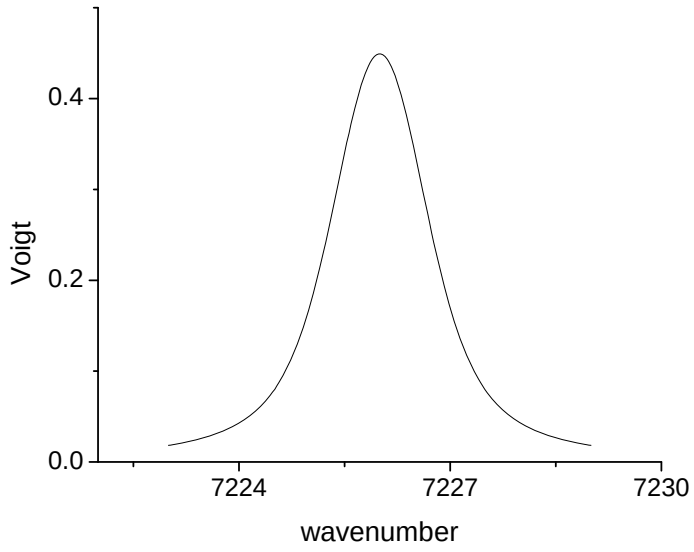


**Figure 8** Origin Voigt curve

To get the coordinates of this curve, we can click on the *analysis* tab, then *fitting*, next *nonlinear curve fit*, and finally *last used*. This will give the coordinates in tabular form. Now these data can be copied into an Excel file to use for the calculation of the absorption coefficient.

To calculate an absorption coefficient at a specific wavelength, we need to go back to the equation

$$k_\nu = S_{lu}\, \Phi_\nu. \qquad (18)$$

We have confirmed that the value in HITRAN is suitable for use for the line strength value. The procedure above allows us to tabulate values for the Voigt function.

By using the methods described in this and the previous chapters, the values for the absorption coefficients were determined for the water absorption line centered at 1383.887nm. Figure 9 shows this plot.

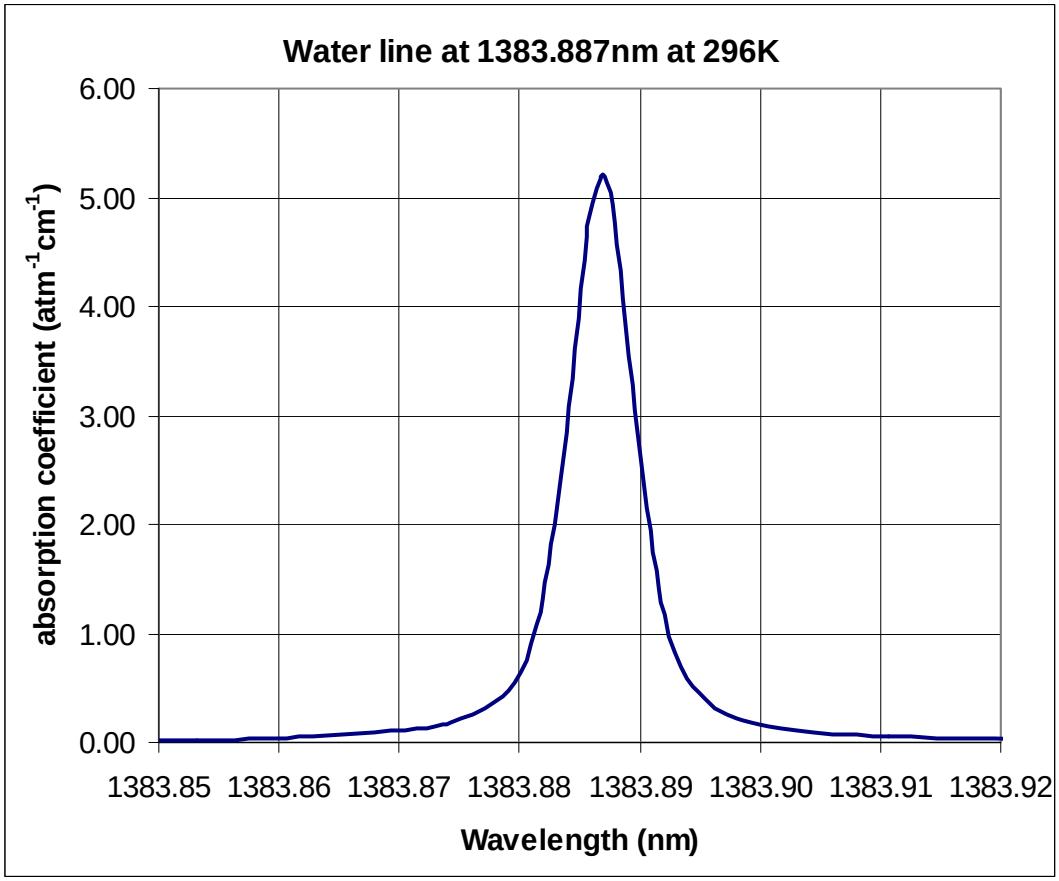


**Figure 9** Absorption coefficient versus wavelength for water vapor at 296K

Another consideration is that since the Voigt function for each individual lineshape will have values at each wavelength, so we will need to add these values together to obtain the final value for the absorption coefficient. This is due to the overlapping of lineshapes from neighboring lines. Although this summation is an absolute necessity when dealing with some wavelengths, the wavelengths used in this thesis have no strong absorption

lines close enough to affect the peak value at the pressure utilized herein. For this work, the water lineshapes at the measured wavelengths were significantly isolated from other lineshapes to be able to ignore the cumulative effects. This fact is known because the calculations were performed, and it was confirmed that this is the case. To further illustrate this point, consider that sometimes there are overlapping lineshapes from neighboring absorption lines. The ultimate effect of a neighboring line is cumulative. This concept is illustrated in Figure 10. Suppose we are interested in the lineshape centered at 7226cm$^{-1}$. The absorption line at 7230cm$^{-1}$ overlaps with the line of concern. Therefore, this results in the absorption spectrum within this range being represented by the sum of the two lines which is represented as a dotted line in the figure.

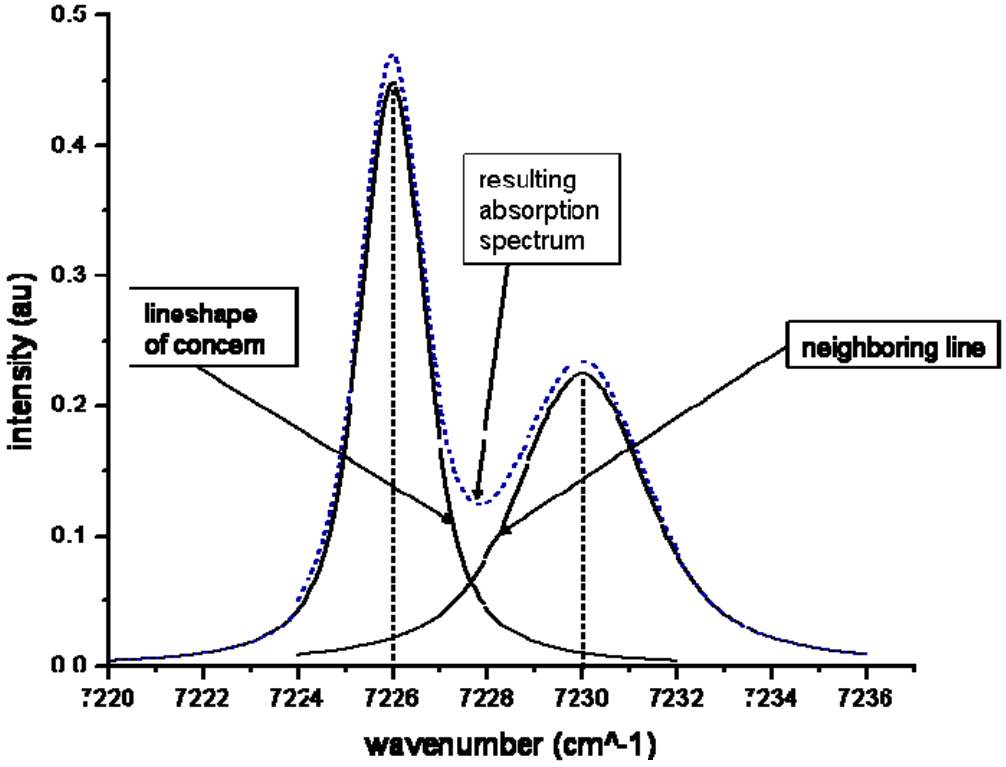


**Figure 10** Cumulative effects of neighboring lineshapes

# CHAPTER IV

# ABSORPTION CELL EXPERIMENTS

The experiments for this work were divided into two parts for the purposes of progressing from simple to more complex considerations. The first part of the experiments, which are described in this section, consisted of an absorption cell being filled with water vapor to a given pressure which was then verified using laser absorption spectroscopy. The procedure, experiment, and results are given for this setup in this chapter. Chapter V describes the second part of the experiment, which consisted of a shock tube being filled with water vapor and Argon gas, a shock being triggered, and the water vapor concentration being determined at three distinct times.

## Procedure

In this section, the setup is described for the experiments which used the absorption cell. The path of the laser is followed from its source, the tunable diode laser, to its final destination, the photoreceiver. Figure 11 gives the layout of the experimental setup with all of the optical components shown.

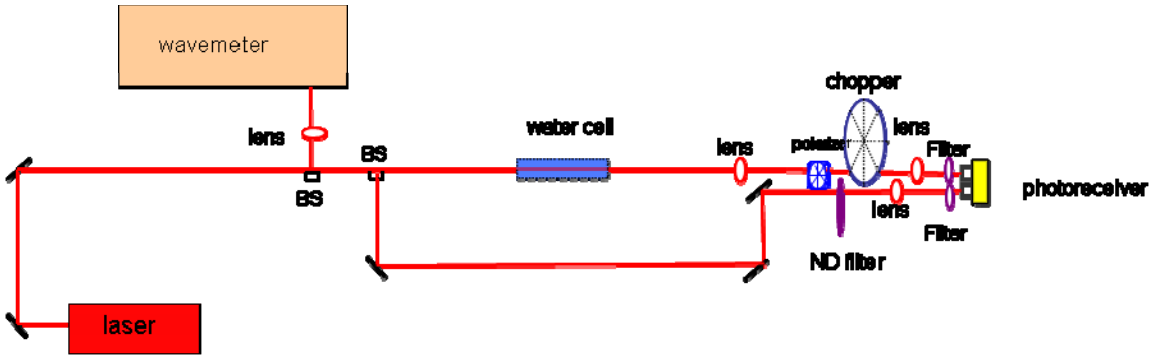


**Figure 11** Schematic of experimental setup for absorption cell experiments

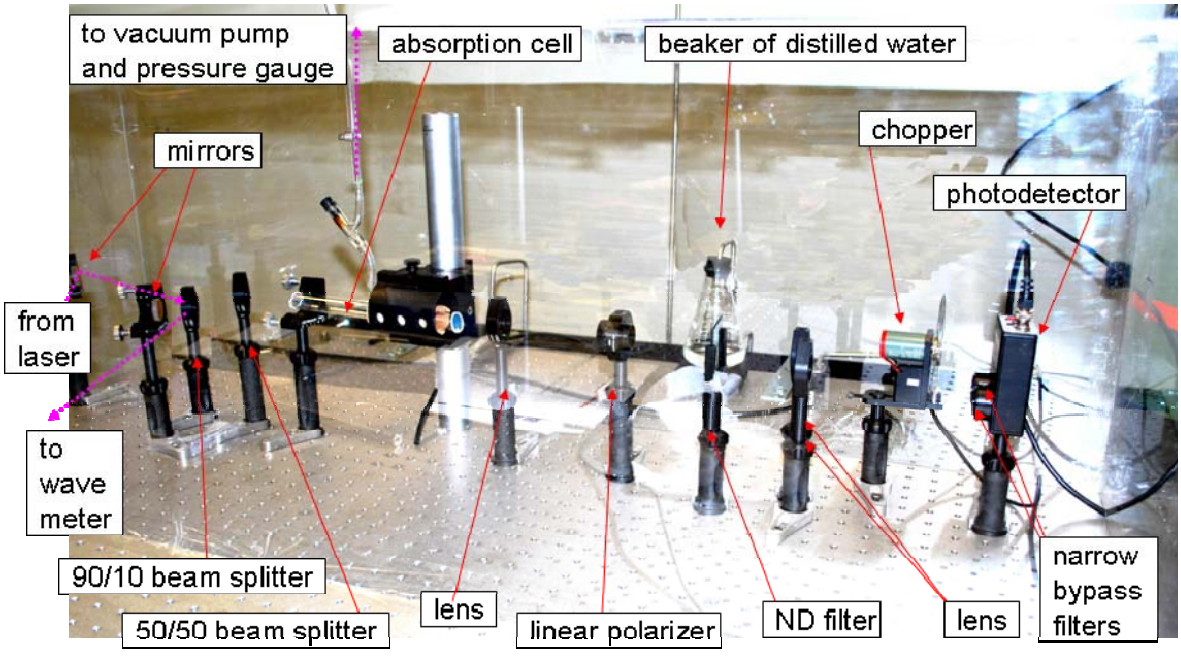


**Figure 12** Photograph of experimental setup for absorption cell experiments

Figure 12 shows a photograph of the actual setup used for the set of experiments described in this section. The dotted pink line shows the incoming laser beam, the split portion of the beam that goes to the wavemeter, and the vacuum line for the absorption cell.

The experimental procedure consisted of setting up the laser in a free beam configuration which was guided with mirrors and optics through an absorption cell (Triad Technologies, TT-H2O-4T-200-Q) filled to a known pressure with water vapor. A schematic of the cell dimensions is given in Figure 13. The cell was constructed of UV-grade fused silica. The windows to the cell were mounted at an angle of 11 degrees.

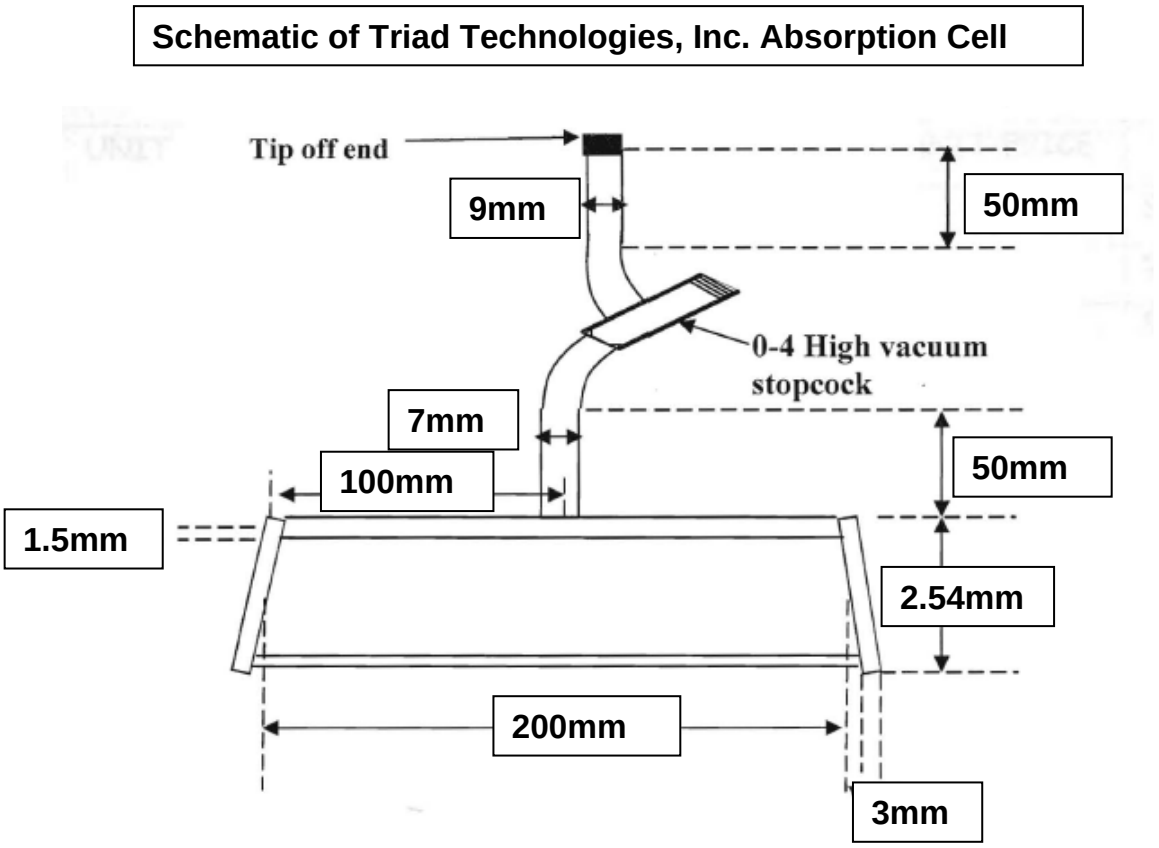


**Figure 13** Schematic of Triad Technologies, Inc. absorption cell utilized in the water cell absorption measurements.

Before the cell was filled with water vapor, it was pumped down to a vacuum using a rotary vane pump (Varian DS420). The vacuum within the cell was then used to vaporize the distilled water within the flask. Once the cell was filled to a suitable pressure, the valve was closed to isolate the cell. In this way, the absorption cell was filled to a known pressure with pure water vapor. The pressure in the cell was kept below 17 torr at 23 degrees Celsius to assure that no condensation occurred.

Figure 14 shows a close-up of the Toptica DL100L tunable diode laser from Toptica Photonics which was used for all experiments performed for this thesis. To tune the laser to a specific wavelength, three controls were used. The coarse tuning was achieved by turning a set screw which controlled the position of the diffraction grating within the laser casing. For fine tuning of the laser, a laser controller (Toptica DC 110) was used to adjust the temperature and/or current. Using these controls, the laser was tuned to specific wavelengths along a known water absorption lineshape centered at 1383.887 nm.

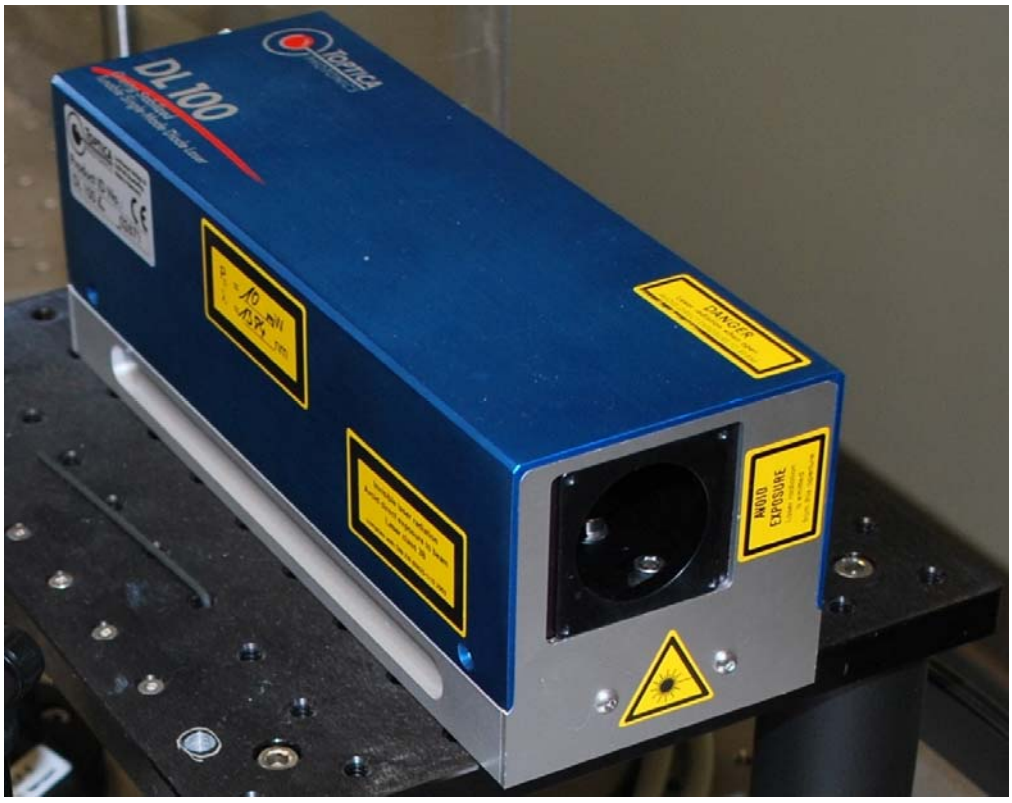


**Figure 14** Photograph of tunable diode laser used for experiments

To eliminate the error associated with room humidity, a purge box was constructed out of 1/16" thick Plexiglas, and the experimental setup was enclosed within it. The box was then purged with dry $N_2$ replacing room air with dry nitrogen. There was a hygrometer

placed within the purge box to measure the relative humidity. Before any experiments were performed, the box was purged with nitrogen for about one hour. This purging procedure allowed the relative humidity to drop below one percent.

The Toptica Photonics tunable diode laser emits light at 1380-1390 nm at a maximum power of about 8mW. All turning and directing of the laser beam was accomplished by using mirrors (Newport Corp., 10D520ER.4). Once initially turned 180 degrees, the beam of the laser was split with a 90/10 beam splitter. The 10% portion of the laser was sent to the wavemeter (Burleigh WA-1000) to measure the wavelength. The 90% portion was directed through the remainder of the experimental setup to be used for absorption purposes. The 90% portion of the laser beam which was used for absorption was sent through the side wall of the purge box and then split with a 50/50 beam splitter (Newport Corp., 10B20BS.3). One leg of the beam goes to the photodetector and the other leg goes through the cell and then to the photodetector. The leg going straight to the photodetector would have no absorption. The leg going through the absorption cell would be attenuated by the absorption of the water vapor. The photodetector measured the difference between the two inputs. By using a chopper and blocking the leg of the beam going through the cell, the incident intensity was able to be obtained, since this would be the intensity of one leg of the beam after going through the 50/50 beam splitter. Prior to filling the cell with water, the two legs of the beam would be balanced to account for any reflections from the cell windows. In other words, the cell is at a vacuum, the two legs of the beam travel their respective paths, and the output of the photodetector gives a difference in

signal intensity of zero. This process also factors out any reflection or attenuation caused by the windows of the absorption cell.

The purge box contained all optics between the 50/50 beamsplitter and the photodetector. The reason that the entire beam was not contained within the purge box was so the volume of the purge box could be minimized. Absorption of the laser intensity will occur from the point the laser light leaves the laser until the point it passes through the purge box. Calculations were performed, and this loss of power was verified to be insignificant. The amount of power lost due to reflection and absorption upon passing through the walls of the purge box was also quantified, and it too was deemed insignificant. Irrespective of these two sources of loss, the laser still supplied sufficient power to perform the experiments, so these losses were not quantified. Ultimately, the most important factor for the laser intensity was that each leg of the beam was balanced once it passes through the 50/50 beamsplitter and that no losses occur in those sections.

After the beam goes through the cell and before it goes to the photodetector, there is a series of optics through which the beam has to travel. Initially, the cell would be empty. There is a rotary vane pump (Varian DS420) which can vacuum the cell down to an ultimate pressure of $10^{-3}$ torr. Therefore, no water vapor will be in the cell. Also, the box enclosing the setup was purged with $N_2$. Both of these procedures are necessary to assure that no absorption is taking place along the measured pathlength of the laser beam.

On the leg of the beam that does not pass through the cell, there was also a set of optics positioned along the beam path. This set of optics focused, attenuated, balanced, and filtered the beam before it arrived at the photodetector. First a lens (Newport Corp., KPX094) was used to focus the beam onto the linear polarizer (Newport Corp., 05LP-NIR). The polarizer can adjust the intensity of the beam and is used to fine tune the balancing of the intensity for the two legs of the beam. There was also a ND filter (Newport Corp., FRQ-ND03) which was used in combination with the linear polarizer to attenuate the beam intensity. This allowed the two legs of the beam to be balanced prior to filling the cell to a given pressure with water vapor and performing absorption spectroscopy. The ND filter is required because the windows of the cell reflect and attenuate light to the extent that the polarizer alone is not enough to attenuate the beam. Once the beam passes through the ND filter, it passes through a second lens. This lens was used to focus the beam onto the sensor of the photodetector that is 3-mm square. Also, there is a narrow-band bypass filter (CVI Laser, F10-1400-5) that restricts the light passing onto the large-area balanced photoreceiver (New Focus, 2317) sensor to 1384 +/- 10 nm.

The output from the photodetector was analyzed using an oscilloscope (Instek, INS GOS-620). The temporal variability of the signal was observed to assess the stability of the output. Once it was ascertained that the output was stable, a voltmeter was used to record the voltage. The chopper was moved to get the complementary voltage reading. This procedure was repeated to verify the repeatability of the measurements. In this way, the incident and transmitted voltage readings were obtained. With these voltage

measurements and the known data from the spectroscopy calculations, the pressure within the cell was able to be determined. This calculated pressure was then compared to the measured pressure which was measured using a pressure transducer.

## Experiment

This section provides the details of the experiments using the absorption cell filled with water vapor and the process used to determine the amount of absorption within the cell using the Beer-Lambert relation and the principles of absorption spectroscopy.

The absorption cell was pumped down to a pressure of 0.004 torr. It was then filled to a pressure of 15.9 torr with water vapor. The laser was tuned to a specific wavelength, and the voltage reading coming from the photoreceiver was recorded for the cell filled with water.

## Results

Once the experiments were performed, the values were used to determine the amount of absorption caused by the water vapor within the cell. These data were then compared to the theoretical values for absorption using the same parameters. Figure 15 shows the results of the absorption cell experiments as a comparison of the measured (experimental) values and the theoretical values.

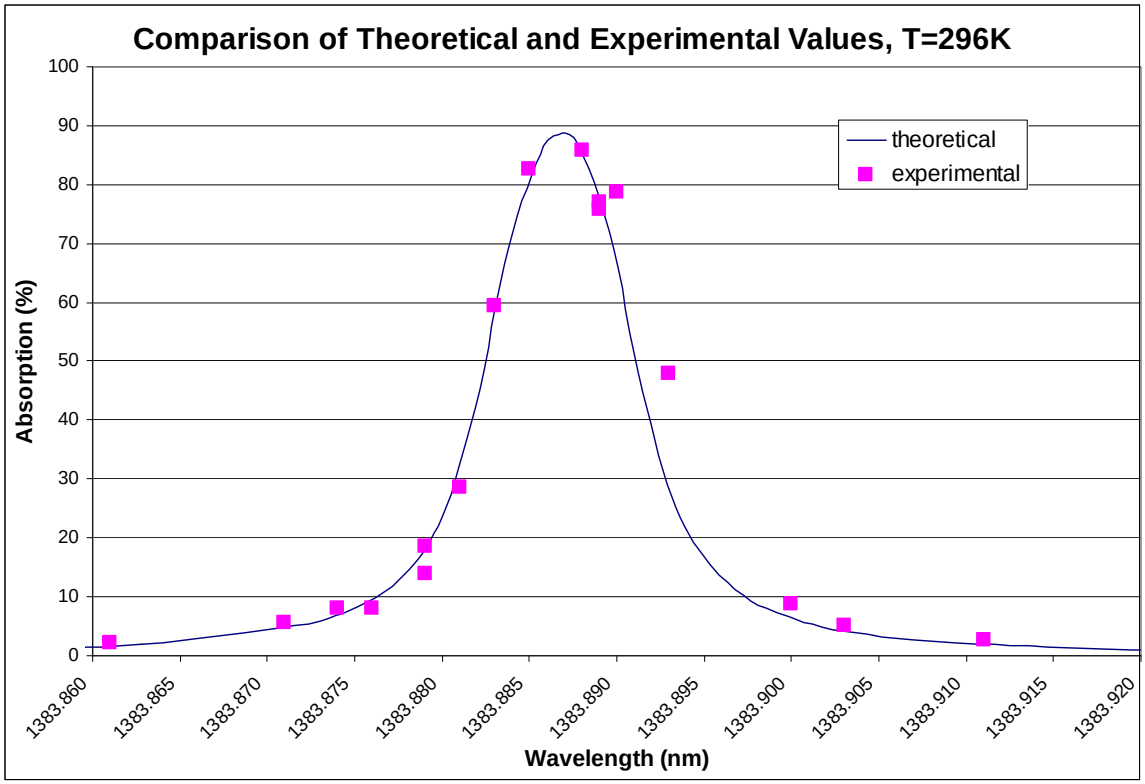


**Figure 15** Comparison of theoretical and experimental values for absorption cell

The results of this set of experiments showed excellent agreement between the theoretical and experimental values. Most of the experimental data agrees within one percent of the theoretical, although there are a few data points that are outside of this range. It is hypothesized that the calculated absorption percentage is correct for these points, but the laser drifted a few thousands of a nanometer is wavelength during the experiment which displaced the point off of the curve. Figure 15 shows the results for twenty measurements. About four of these measurements are beyond the one percent error range due to drifting of the laser. This uncertainty can be corrected in future experiments and will be discussed in chapter VIII: Recommendations. This satisfactorily concludes the

absorption cell experiments. In the next chapter, absorption within the shock tube is discussed.

# CHAPTER V

# SHOCK-TUBE EXPERIMENTS

The next part of the experiment consists of a shock tube being used as the vessel to contain the water vapor and as a means to heat the water to high temperatures. The shock tube was filled with a mixture of water vapor and Argon, a shock was triggered, and the water vapor concentration was determined at three distinct times- before the incident shock, after the incident shock but before the reflected shock, and after the reflected shock. Argon was added as an inert gas which allowed the partial pressure of the water to remain below its vapor pressure while allowing the shock tube to be filled to the required pressure needed to get a suitable pressure and temperature for the test conditions.

## Procedure

In general, the experimental setup for the shock tube was very similar to the setup for the absorption cell. The differences between the two setups are noted below in lieu of rewriting the entire procedure. Figure 16 shows a schematic of the experimental setup for the shock-tube experiments.

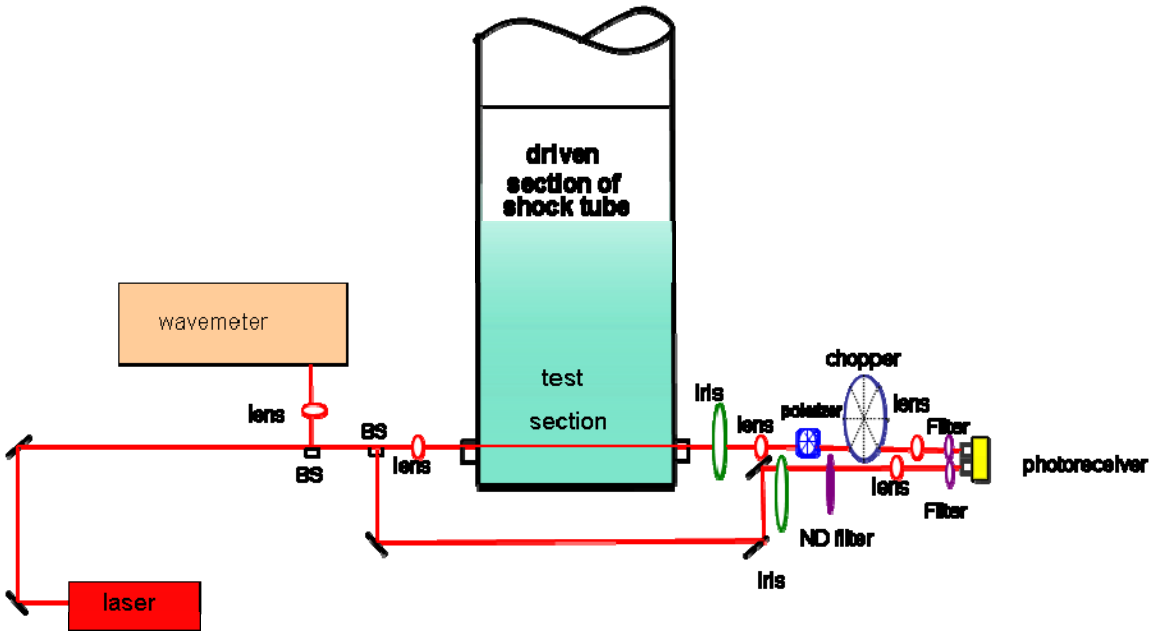


**Figure 16** Schematic of experimental setup for shock-tube experiments

Figure 17 shows a photograph of the experimental setup for the shock-tube experiments.

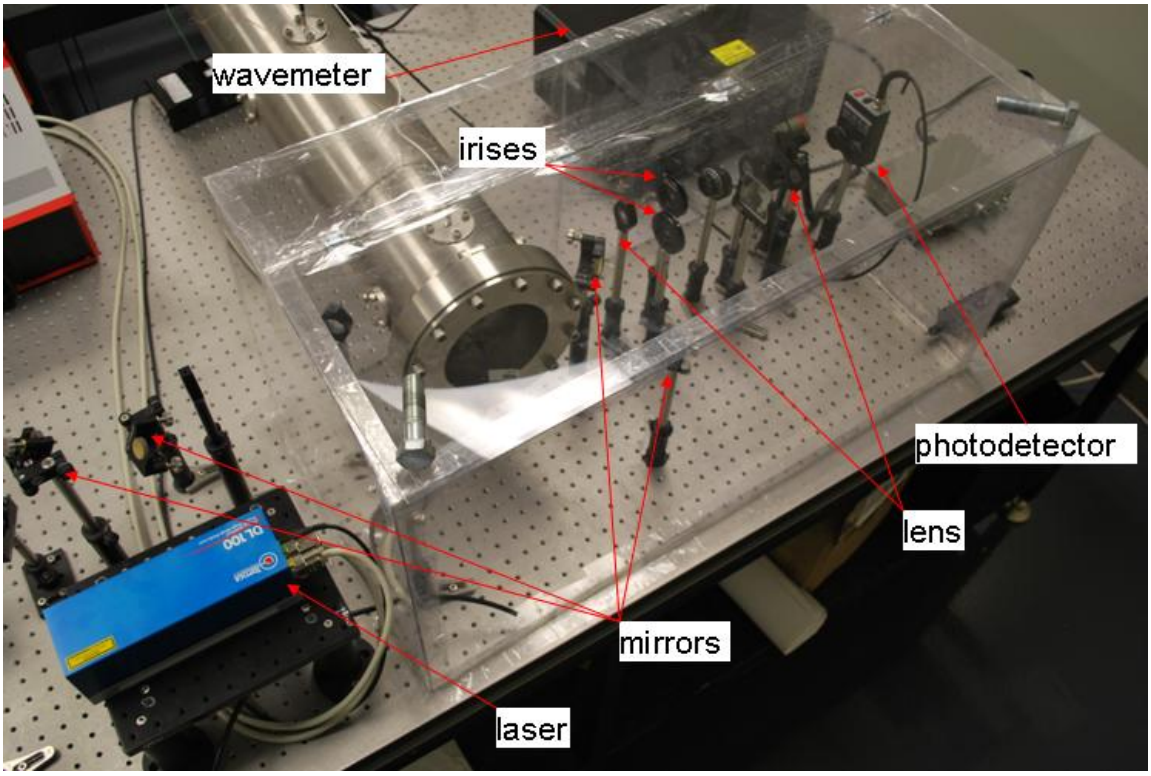


**Figure 17** Photograph of experimental setup for shock-tube experiments

The major (and obvious) difference between the two setups is that for this set of experiments, instead of sending the laser through an absorption cell, it was sent through a shock tube. The shock tube used for this work has been detailed by Aul et al., and a schematic of it is shown in Figure 18 [22].

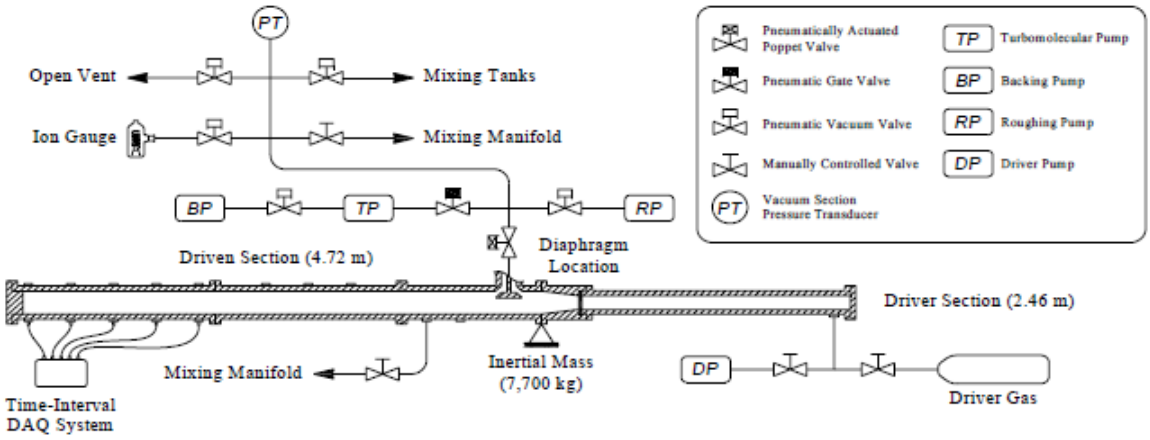


**Figure 18** Shock tube at Texas A&M University

A shock tube is an apparatus which consists of two sections of metal tube connected by a diaphragm which is broken to produce an elevated temperature in the test section portion of the tube by sending a shockwave down the tube. The shock tube at Texas A&M University has a driver section that is 2.46 meters long and a driven section that measures 4.72 meters. This device can be used to obtain reflected-shock conditions of over 50 atmospheres and 2000 K.

A brief outline of the operating procedure is discussed as follows for the uninformed reader. First, a lexan (or aluminum for higher pressures) diaphragm is inserted between the two sections. Next, both sections of the shock tube are pumped down. The driven section is pumped down to an ultimate pressure of $1 \times 10^{-6}$ or lower through the use of a Varian DS420 roughing pump and a Varian 551 turbo-molecular pump. The driver section is pumped using a Varian DS102 roughing pump. The driven section is then filled with the test gases. In this work, water vapor and Argon gas were used. Next, the

driver section is filled with a driver gas (usually Helium) until the diaphragm bursts, sending a shockwave down the tube. As governed by the Rankine-Hugeniot shock relations, the pressure ratio across the diaphragm determines the intensity of the shock which in turn determines temperature ratio across the shock. In this way, the shockwave is used to increase the temperature behind its forward moving face. The shock travels the length of the driven section and when it reflects off the end wall, the temperature is once again increased giving the test conditions.

Another important difference between the two setups was that for the shock-tube experiments an iris (Newport Corp., ID-1.0) was set up as the first optical component on both the incident and transmitted legs of the laser beam leaving the shock tube. The reason that an iris was inserted for the shock-tube experiments is that black body radiation from the hot gases may skew the readouts of the intensities from the photodetector. By inserting an iris, any stray interference radiation is greatly reduced.

Figure 19 shows a photograph for the shock-tube setup illustrating the major components including the shock tube, laser, laser controller, wavemeter, and purge box. As can be seen in this photograph, most of the optics are contained within the purge box, but some are outside of it. The laser beam is steered using mirrors and then split with the 90/10 beamsplitter to enable the wavemeter to determine the wavelength. The larger intensity portion of the beam is directed through the wall of the purge box where it is then split with the 50/50 beamsplitter and directed through the remainder of the optics. As mentioned previously, the only difference in the beam path after the 50/50 split is that the

absorption cell has been replaced with the shock tube and that an iris has been added to each leg immediately behind the shock tube.

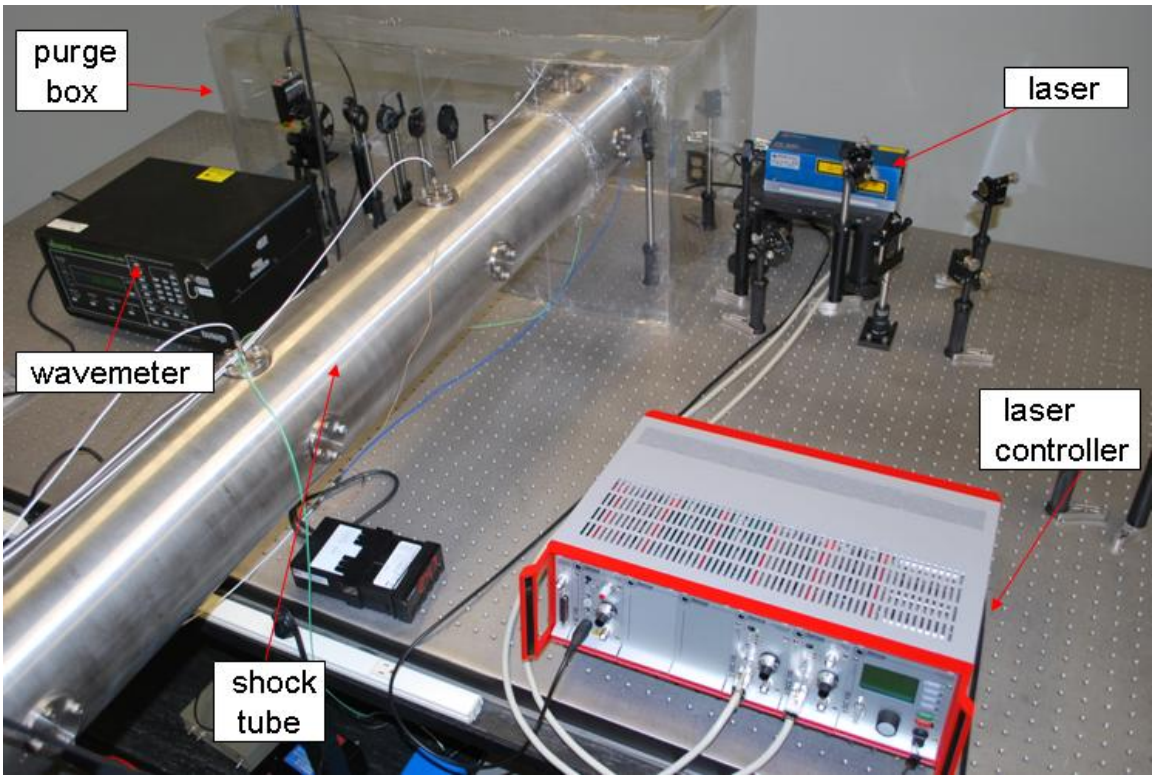


**Figure 19** Photograph of experimental setup for shock-tube experiments

To achieve the proper temperature and pressure values in the test section, the shock tube had to be filled to about one atmosphere. Since the vapor pressure of water is 21.07 torr at 23 degrees Celsius [23], argon was added to water vapor before filling the shock tube. This prevented condensation of the water vapor. The best way to achieve the mixture of argon and water vapor was to add water vapor to a mixing tank then add the argon to it. This mixture was thoroughly mixed during the process of adding the argon due to a multi-holed sting running the length of the mixing tank which allowed turbulent mixing

of the two gases since the gases are introduced via the resulting jets from the multiple holes.

The output from the photoreceiver was recorded using a GageScope DAQ board and a desktop computer.

**Experiment**

Three runs were performed in the shock tube. Each of these runs was filled to the same initial pressure. Since the diaphragm broke at about the same pressure each time, this same value for the fill pressure enabled the temperatures in the test section after the incident and reflected shocks passed to be repeatable. The temperature after the passing of the incident shock is known as $T_2$ and was about 1060 K. The temperature after the passing of the reflected shock is known as $T_5$ and was about 2000 K.

**Results**

Once the experiments were performed, the values were used to determine the amount of absorption caused by the water vapor within the shock tube. These data were then compared to the theoretical values for absorption using the same parameters. Figure 20 shows the results of the experiments as a comparison of the experimental values and the theoretical values at room temperature.

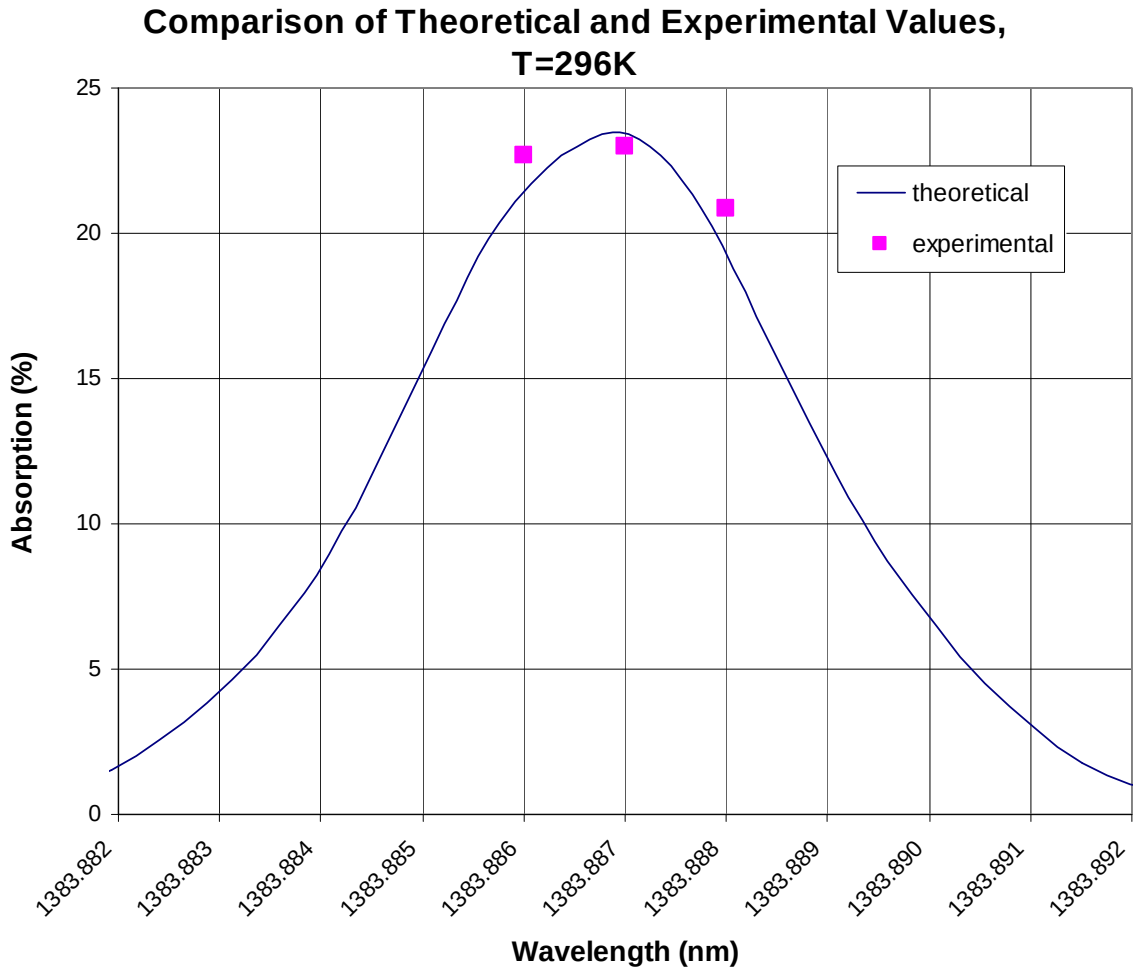


**Figure 20** Comparison of theoretical and experimental values for shock-tube experiments at the initial fill condition, T = 296K

Figure 21 shows the results of the experiments as a comparison of the experimental values and the theoretical values after the incident shock passed through the test section. The temperature at these conditions was 1060 K.

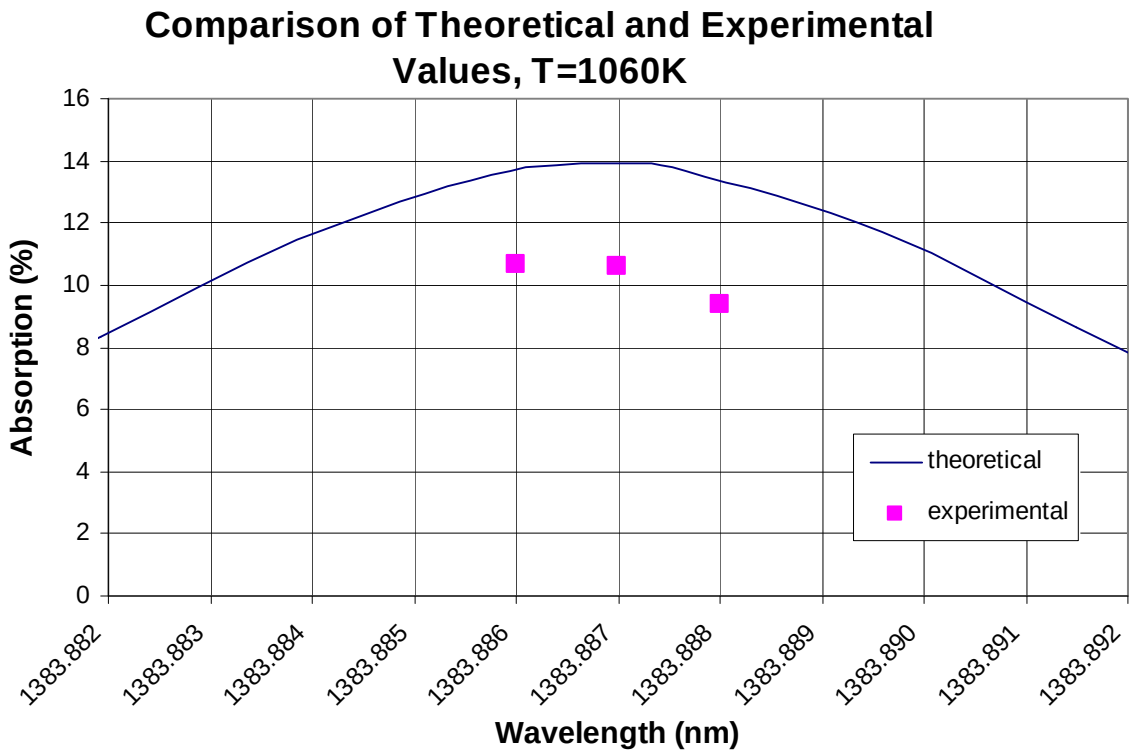


**Figure 21** Comparison of theoretical and experimental values for shock-tube experiments after passage of the incident shockwave, at T=1060K

Figure 22 shows the results of the experiments as a comparison of the experimental values and the theoretical values after the reflected shock passed through the test section. The temperature at these conditions was 2000 K.

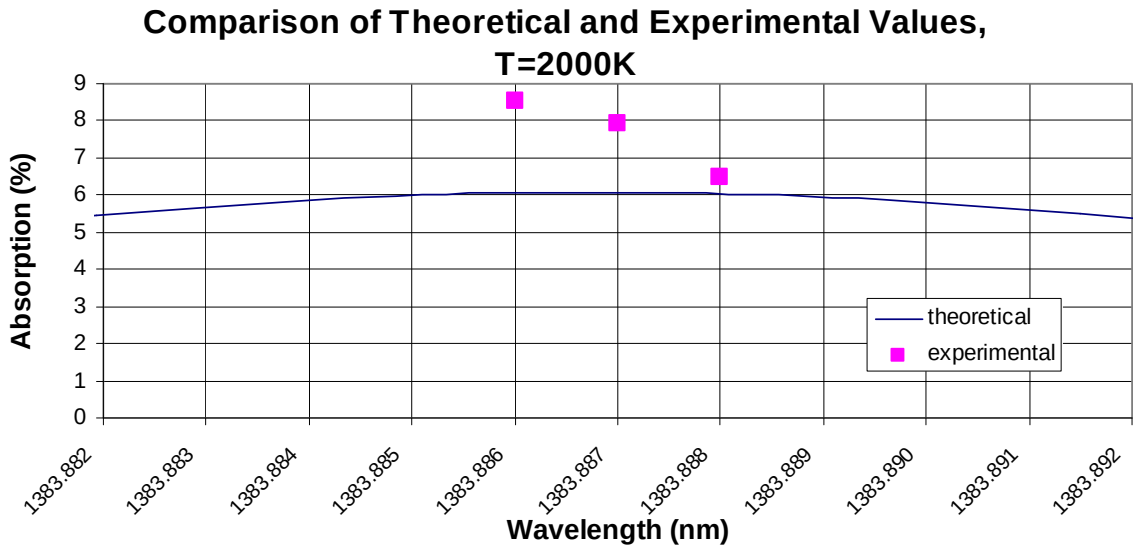


**Figure 22** Comparison of theoretical and experimental values for shock-tube experiments at T=2000K

Figure 23 shows a plot of the output voltage for the pressure trace and for the photoreceiver. It can be seen that as the incident wave passes, an increase in pressure is observed. Another increase is pressure occurs as the shock wave hits the end wall of the shock tube and reflects back down the tube. Figure 23 also shows the voltage readout for the photoreceiver. From the plot, it's noted that as each shock wave passes through the mixture of gases contained within the shock tube, a change in the differential output voltage of the photoreceiver occurs. This change in voltage is indicative of a change in absorption due to the changes in pressure and temperature.

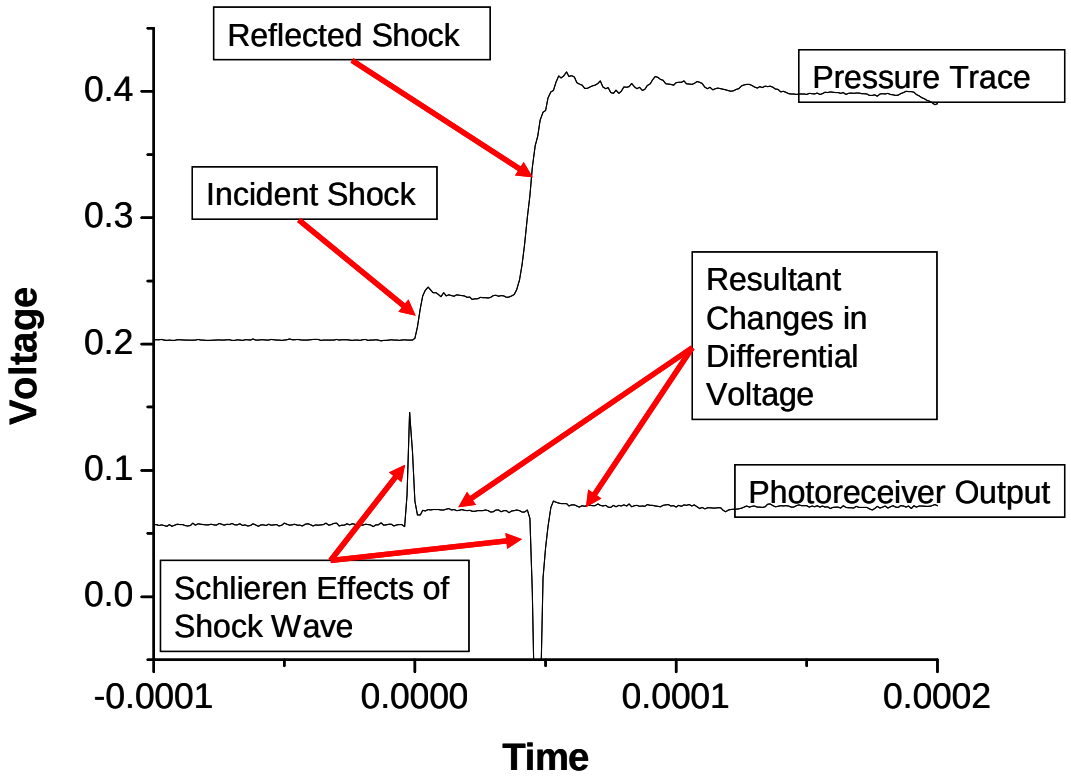


**Figure 23** Pressure trace and photoreceiver output for typical shock-tube run

A point of interest is figure 23 is the spikes that occur in the voltage output of the photoreceiver. These spikes are due to the Schlieren effect which stated simply is due to light inflexions due to optical artifacts. As the shock passes, the sudden change in pressure and temperature causes the Schlieren effect and results in a voltage spike. This spike may be positive or negative.

The results for the shock-tube experiments at room temperature show good agreement between the theoretical and experimental data. The results for the shock-tube experiments at elevated temperature show a reasonable degree of agreement between the

theoretical and experimental data. The agreement is not as close as the absorption cell experiments.

# CHAPTER VI

# SUMMARY AND CONCLUSION

## Summary

For this thesis, the Beer-Lambert relation was used to calculate absorption percentage given the concentration of water. The correlation between species concentration and absorption is known, and if one is known the other can be calculated.

## Conclusion

The data for the absorption cell experiments show excellent agreement with the theoretical calculations. Most of the experimental data agree within less than one percent of the theoretical data. Laser drift may account for any errors of greater than one percent in these runs.

For the shock-tube data, there is some disparity in the comparison between the experimental and theoretical values. At room temperature, there is a small margin between the two sets of values. For the sets of data at elevated temperature, there is a somewhat larger discrepancy.

One major contributing factor in the shock-tube runs may be due to the drift of the laser during the experiment. In these experiments, the laser was tuned to a desired wavelength, and then two legs of the laser were balanced prior to filling the shock tube. The shock tube was then filled with the argon/water vapor mixture. During the filling, the laser had an increased period of time (compared to the absorption cell experiments) in which drift may have occurred. For the absorption cell experiments, once the laser was tuned, the

cell was filled and the measurements taken within 60-90 seconds. For the shock-tube experiments, this time was on the order of 12-15 minutes. This increase in time duration may have allowed the laser to drift to another wavelength or even to have modehopped. A drift in the laser could have changed the wavelength be several thousand nanometers. If the laser modehopped, it could have changed by hundredths of nanometers, tenths of nanometers, or even one or more nanometers while the shock tube was being filled.

# CHAPTER VII

# RECOMMENDATIONS

Since the laser has a tendency to drift during the experiments, it is suggested that a way to lock the laser to a desired wavelength is implemented. There are several ways to accomplish this.

Laser drift is caused by fluctuation in the injection current, temperature, and mechanical fluctuations. The laser drift can be stabilized by locking it to an external reference. Laser frequency stabilization is based on generating a frequency error signal.

Frequency locking of a laser is often done by using a narrow peak in a saturated absorption spectrum as an external reference. The laser frequency is tuned to either the side of the absorption line or its peak. Side-locking is one of the simplest methods and entails locking the laser to the side of the absorption line. Some drift may still occur using this method. Peak- locking uses the peak absorption and is less susceptible to drift than the side-locking method. Other locking methods are possible and should be investigated and implemented to decrease uncertainty in the wavelength of the laser. [25]

# REFERENCES

[1] Eckbreth, A. C., *Laser Diagnostics for Combustion Temperature and Species*, *Energy and Engineering Science Series*, Vol. 7, Abacus Press, Cambridge, Mass, 1988.

[2] Linne, M. A., *Spectroscopic Measurement*, *An Introduction to the Fundamentals*, Academic Press, New York, 2002.

[3] http://en.wikipedia.org/wiki/Laser, "Laser," accessed Nov. 11, 2009.

[4] http://en.wikipedia.org/wiki/Stimulated_emission, "Stimulated Emission," accessed Nov. 11, 2009.

[5] Fadini, A., and Schnepel, F.-M., *Vibrational Spectroscopy*, *Methods and Applications*, English Edition, Ellis Horwood Limited, 1989.

[6] Pinta, M., *Atomic Absorption Spectrometry.* English Edition, Adam Hilger Ltd., London, 1975.

[7] Herzberg, G., *The Spectra and Structures of Simple Free Radicals, An Introduction to Molecular Spectroscopy* Cornell University, New York, 1971.

[8] Vincenti, W.G., and Kruger, Jr., C.H., *Introduction to Physical Gas Dynamics*, Robert E. Krieger Publishing Co., Inc., Florida, 1986.

[9] http://www.originlab.com/, "Data Analysis and Graphing Software," accessed Nov. 11, 2009.

[10] Steinfeld, J.I., *Molecules and Radiation, An Introduction to Modern Molecular Spectroscopy*, MIT Press, New York, 1978.

[11] Di Rosa, M.D., "High-Resolution Line Shape Spectroscopy of Transitions in the Gamma Bands of Nitric Oxide," HTGL Report T-327, May 1996.

[12] http://en.wikipedia.org/wiki/Planck_constant, "Planck Constant," accessed Nov. 11, 2009.

[13] Arroyo, M. P. and Hanson, R K., "Absorption measurements of water-vapor concentration, temperature, and line-shape parameters using a tunable InGaAsP diode laser," *Applied Optics*, Vol. 32, No. 30, Oct. 1993, pp. 6104-6116.

[14] http://www.cfa.harvard.edu/hitran//, "The HITRAN Database," accessed Nov. 11, 2009.

[15] Wang, L.-G., Tate, D. A., Riris, H. and Gallagher, T. F., "High-sensitivity frequency-modulation spectroscopy with a GaAlAs diode laser," *J. Opt. Soc. Am. B 6*, 1989, pp. 871-876.

[16] Goldstein, N., Adler-Golden, S., Lee, J., and Bien, F., "Measurement of molecular concentrations and line parameters using line-locked second harmonic spectroscopy with an AlGaAs diode laser," *App. Opt. 31*, 1992, pp. 3409-3415.

[17] Carlisle, C. B. and Cooper, D. E., "Tunable diode laser frequency modulation spectroscopy through an optical fiber: high sensitivity detection of water vapor," *Appl. Phys. Lett. 56*, 1990, pp. 805-807.

[18] Stanton, A.C., Bomse, D. S. and Silver, J. A. "A nonintrusive diagnostic for water vapor in high temperature flow fields," Tech. Rep. R90-01, for National Aero-Space Plane Joint Program Office AFSC/NAC (Southwest Sciences, Inc., Santa Fe, NM, 1991).

[19] Nagali, V., Herbon, J., Horning, D., Bates, R., Davidson, D. F. and Hanson, R. K., "Diode-Laser Based Diagnostic to Monitor Water-Vapor in High-Pressure Environments," *37th AIAA Aerospace Sciences Meeting and Exhibit*, AIAA Paper 99-0942, 1999.

[20] Di Rocco, H. O., "The exact expression of the Voigt profile function," *Journal of Quantitative Spectroscopy & Radiative Transfer 92*, 2005, pp. 231-237.

[21] Roston, G. D. and Obaid, F. S., "Exact analytical formula for Voigt spectral line profile," *Journal of Quantitative Spectroscopy & Radiative Transfer 94*, Vol 94, 2005, pp. 255-263.

[22] Aul, C.J., de Vries, J., and Petersen, E.L., "New Shock-Tube Facility for Studies in Chemical Kinetics at Engine Conditions," 5th US Combustion Meeting, Oct. 2007.

[23] Cengel, Y.A. and Boles, M.A., "Thermodynamics," *An Engineering Approach*, 4th ed., McGraw-Hill, New York, 2002, pp. 830.

[24] Dias, A.C.B., Borges, E.P., Zagatto, E.A.G. and Worsfold, P.J., "A critical examination of the components of the Schlieren effect in flow analysis," *Talanta: Journal of Analytical Chemistry*, published online 30 Nov. 1989; Vol. 68, No. 4, 2006, pp. 1076-1082.

[25] http://electron9.phys.utk.edu/optics507/modules/m10/diode_laser_frequency_stabilizat.htm, "Diode Laser Frequency Stabilization," accessed Nov. 11, 2009.

# VITA


| | |
|---|---|
| Name: | Alexander Bertram Barrett |
| Address: | Department of Mechanical Engineering, 3123 TAMU, Texas A&M University, College Station, TX 77843 |
| Email Address: | alexanderbb2003@yahoo.com |
| Education: | B.S., Aerospace Engineering, University of Central Florida<br>M.S., Mechanical Engineering, Texas A&M University |